Pergamon

PII: S0022-3697(96)00229-6

J. Phys. Chem Solids Vol 58, No. 7, pp. 1167–1172, 1997

0022-3697/97 $17.00 + 0.00

IN SITU ESR STUDY OF THE HNO_3-INTERCALATE DIFFUSION PROCESS IN GRAPHITE INTERCALATION COMPOUNDS

A. M. ZIATDINOV and N. M. MISHCHENKO

Institute of Chemistry, Russian Academy of Sciences, 100-let Vladivostoku, 159, 690022 Vladivostok, Russia

(*Received* 28 *May* 1995; *accepted* 31 *May* 1995)

Abstract—*In situ* conduction electron spin resonance (CESR), contactless conductivity and X-ray diffraction studies of HNO_3 molecule intercalation into highly oriented pyrolytic graphite (HOPG) plates are presented. The CESR lineshape, linewidth, intensity and position analysis allow us to establish: a) individual reaction steps, b) two different intercalation mechanisms: a slow diffusion of the intercalate through faces parallel to the *c*-axis in the whole thickness of a sample and a relatively faster nucleation of a new phase in near surface galleries; and c) an estimate of the constant of the two-dimensional diffusion of intercalate through the sample after its insertion into HOPG. Each of the intercalation mechanisms is characterized by an 'induction period', in which the graphite takes up comparatively little intercalate, and by an index of the stage appearing on its own.

Keywords: A. metals, B. chemical synthesis, C. grain boundaries, D. order–disorder effects, E. electron paramagnetic resonance.

INTRODUCTION

Graphite intercalation compounds (GICs) are two-dimensional synthetic metals and consist of an alternating sequence of n hexagonal graphite monolayers (where n is the stage index) and a monolayer of foreign atoms or molecules (the intercalate) [1]. In spite of numerous publications devoted to studies of various aspects of GIC structure and properties, until recently the mechanism of intercalation of 'guest' molecules has not received sufficient attention. Only a few conduction electron spin resonance (CESR) studies of GIC kinetics and diffusion have been undertaken [2–6]. In ref. [6] we presented the results of a new procedure for *in situ* CESR studies of the SbF_5 molecule intercalation process into highly oriented pyrolytic graphite (HOPG). This paper is devoted to the results of further *in situ* CESR studies of intercalation of HNO_3 molecules into HOPG, as well as a new presentation of the reasons for the CESR lineshape transformations observed with HNO_3 molecule intercalation. A data comparison for *in situ* basal plane electrical conductivity σ_a and the X-ray diffraction picture vs exposure time (τ) of the system (HOPG + HNO_3) is also presented.

EXPERIMENTAL

CESR measurements were carried out at room temperature using an X-band E-line spectrometer. The constant magnetic field (H_o) modulation frequency and amplitude were 2.5 kHz and 0.1 mT, respectively. The HOPG samples were held in a quartz tube connected via a valve to the reservoir with the intercalate (liquid HNO_3 with the density of $\sim$1.565 g cm^{-3}). Prior to the experiment, the system was evacuated to eliminate air and water. The experiments were carried out on two HOPG plates of rectangular parallelepiped shape with (sample 1): height (h) = 0.4 cm, width ($l = l_1$) = 0.4 cm and thickness ($d = d_1$) = 0.026 cm, and with (sample 2): h = 0.4 cm, $l = l_2$ = 0.04 cm and $d = d_2$ = 0.01 cm, where $l \times h$ are the dimensions of the basal plane. During the measurements H_o was applied along the HOPG plate *c*-axis. The basal ($1 \times h$) and lateral sides ($d \times h$) were parallel to the magnetic component (H_{rf}) of the microwave field (MWF). Note that in the rectangular resonator, the structure of the electromagnetic field of the TE_{102} mode has such a form that, at a conventional setting of the resonator, H_o is parallel to the electrical component (E_{rf}) of the MWF.

In situ σ_a measurements of the HOPG + HNO_3 system were carried out by the contactless Wien bridge method described in ref. [7]. According to this method, σ_a is equal to 1.2×10^4 $(\Omega\,\text{cm})^{-1}$ for HOPG plates at 300 K. According to ref. [8], $\sigma_c = 7.7$ $(\Omega\,\text{cm})^{-1}$ for HOPG plates at the same temperature. This fact implies that $l_1 \gg \delta_c$ and $l_2 \sim 2\delta_c$ (where δ_c = 0.0192 cm is the classic skin-depth governed by σ_c conductivity in the X-band). *In situ* observations of

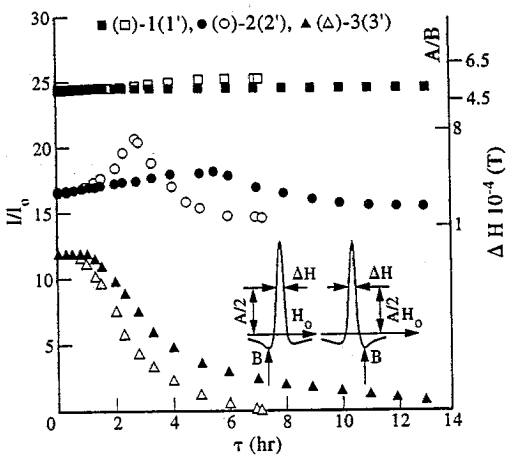

Fig. 1. CESR lineshape parameters of unintercalated parts of sample 1 vs exposure time (τ) in HNO_3 atmosphere. 1(1'), 2(2') and 3(3') correspond to ΔH, A/B and I/I_o, respectively, for plate with protected (unprotected) basal planes. $I = (A + B)\Delta H^2$; I_o is the intensity of the Mn^{2+} ESR line in a standard sample ($ZnS:Mn^{2+}$); $\nu = 9.5$ GHz; $T = 300$ K; $c||H_o, \perp [E_{rf} \times H_{rf}]$.

the stage domain evolution during the intercalation process were carried out by the (001) X-ray diffraction method.

The sizes of the HOPG plates in both the σ_a conductivity and X-ray diffraction measurements were the same ($h \times l \times d = 0.4 \times 0.4 \times 0.026\,cm^3$). The experimental conditions of the intercalation process were similar in both cases.

RESULTS

The HOPG sample resonance line for $H_o||c$ is characterized by $g_{||} = 2.0474 \pm 0.0002$. The line is of an asymmetric shape defined by the Dyson mechanism [9]. The line asymmetry (A/B) is determined as the maximum/minimum peak height ratio, both measured with respect to the base-line of the resonance derivative. The A/B ratio (equal to ~3.4 for sample 1 and ~1.8 for sample 2) for the pure initial HOPG plates is 'normal' in the sense that the maximum peak height occurs at smaller magnetic fields.

In time τ_i (the 'induction' time of the reaction) after the injection of HNO_3 gas into the part of reactor with the HOPG plate, the CESR line of graphite begins to transform and decrease in intensity until it fully disappears (Fig. 1). Simultaneously, in the spectrum a new resonance signal with $g^*_{||} = 2.0019 \pm 0.0002$, and $g^*_{\perp} = 2.0030 \pm 0.0002$ appears, where $g^*_i (i = ||, \perp)$ is determined by the H_o value at the point of insertion of the first derivative of the CESR absorption line and the base-line.

At a given basal plane area and the same other experimental conditions, the length of the 'induction' period depends on plate thickness and increases up to (or decreases down to) its high (low) limit value ~1.5 h (~0.7 h), as the value of d increases (decreases).

At $t > \tau_i$, (~1 h) the A/B ratio of the graphite CESR line of sample 1 increases initially, but it is still 'normal' reaching a maximum value of $A/B \sim 7.2$. Later, upon further exposure to the intercalate atmosphere, the A/B ratio is 'reversed' (maximum peak height occurs at higher magnetic fields), and its magnitude decreases down to ~2; the A/B maximum corresponds to the moment when the phase reversal takes place (see Fig. 1).

In sample 1 over time $\Delta\tau_1$ (~20 h) from the beginning of the reaction, the linewidth of the signal with g^* remains constant (Fig. 2(a)). The increase of the signal integral intensity $I^* = (A^* + B^*)\Delta H^{*2}$, which was observed at the beginning of intercalation, finished at time $\Delta\tau_2$ (~4.5 h) (Fig. 2(a)). At time $\Delta\tau_3$ (~12.5 h), the $A^*/B^*(t)$ dependence passes through a maximum which is equal to 2.1 ± 0.1 (Fig. 2(a)). After time $\Delta\tau_1$ the integral intensity and linewidth rapidly begin to increase and to decrease, respectively. In this time range the A^*/B^* ratio increases to 3.2 ± 0.1 (Fig. 2(a)).

The evolution of the lineshape of the signal with g^* in sample 2 essentially differs from that in sample 1 (Fig. 2(b)). Early in the development of the reaction, a wide scatter of the I^* and ΔH^* values is seen. As the time increases, this scatter decreases and both the I^* and ΔH^* vs exposure time dependences take a clearly defined stepwise form (Fig. 2(b)). During the intercalation the A^*/B^* ratio remains constant.

The CESR spectrum evolution of the (HOPG + HNO_3) system in sample 1 with protected (by the use of bifluoride oil) basal planes shows some peculiarities (Fig. 1). First, the phase of the CESR lineshape is not 'reversed' in spite of the A/B dependence passing through a maximum ~5.0. Second, after the maximum the A/B ratio decreases to 2.7 ± 0.1 and does not change up to the end of this reaction step. Third, in plates with protected basal planes, the time for graphite CESR signal observation is about twice that in plates with unprotected basal planes (when other experimental factors are the same).

The (001) X-ray diffraction study of the HOPG sample with unprotected basal planes at $t < \tau_i$ shows the presence of additional (relative to the pure graphite diffractogram) reflections (Fig. 3(b)). These reflections correspond to GIC with $n > 18$. Near surface plate splitting along the basal plane shows the absence of such additional reflections from the inside part of the HOPG plate and the invariable X-ray diffraction picture from the near surface parts of the HOPG plate, the thickness of which was less than 3×10^{-3} cm. After completing the induction period the intensity of the HOPG and additional reflections

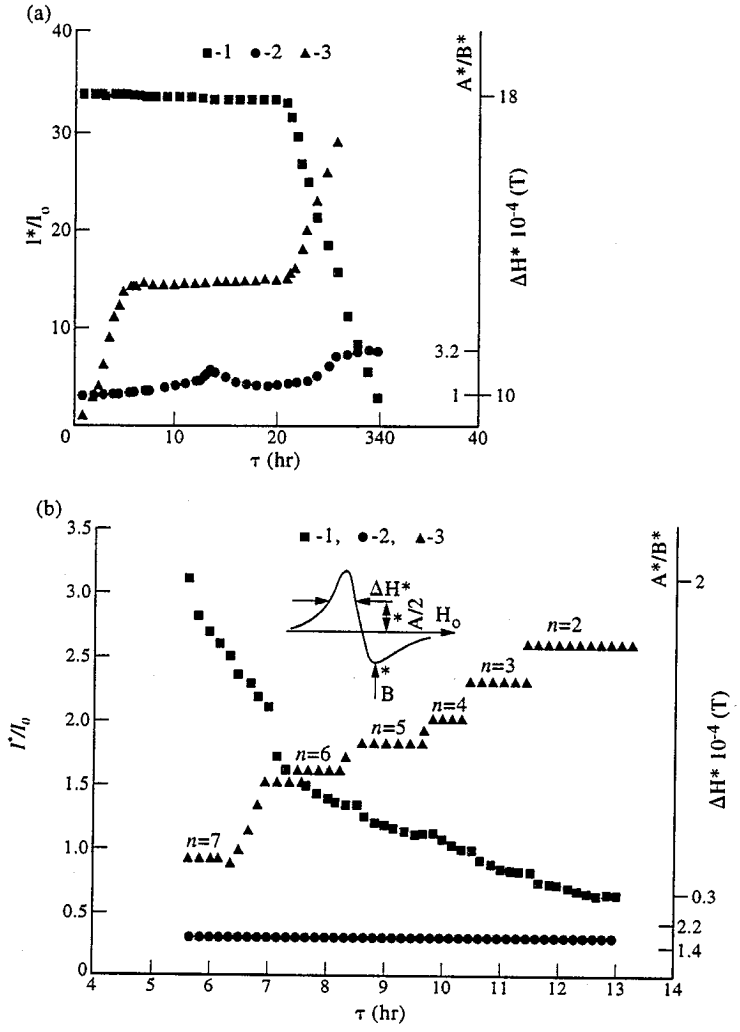

Fig. 2. CESR lineshape parameters of intercalated parts of sample 1 (a) and sample 2 (b) vs exposure time (τ) in HNO_3 atmosphere. 1, 2 and 3 correspond to ΔH, A/B and I/I_o, respectively. $I = (A + B)\Delta H^2$; I_o is the intensity of the Mn^{2+} ESR line in a standard sample ($Zn : Mn^{2+}$); $\nu = 9.5$ GHz; $T = 300$ K, $c||H_o$, $\perp [E_{rf} \times H_{rf}]$.

decreases, and new reflections corresponding to the seventh stage appear (Fig. 3(c)). At the time corresponding to the end of the first plateau of $I^*(t)$ and $\Delta H^*(t)$ dependences (Fig. 2(a)), the seventh stage reflections remain dominant, but in the diffractogram sixth stage reflections of low intensity are also present (Fig. 3(d)). Then fifth stage reflections with growing intensity appear and, simultaneously, the higher stage reflections disappear (Fig. 3(e)), and so on, up to the formation of the stable picture of the fourth stage compound reflections (Fig. 3(f)). In plates with protected basal planes in the induction period only, (001) X-ray reflections corresponding to pure HOPG are registered.

The (001) X-ray diffractograms of sample 2 at a time corresponding to any plateau of the $I^*(t)$ dependence correspond to the pure GIC stage. The stage index decreases from 7 to 2, as the reaction time increases (Fig. 2(b)).

The $\sigma_a(\tau)$ dependence, which has a two-stepwise form, is similar to that of $I^*(t)$ (Fig. 4). The induction period of $\sigma_a(t)$ dependence is approximately equal to 0.7 h.

DISCUSSION

It is evident that in general the HNO_3 molecules may intercalate into HOPG in the form of: 1) separate molecules; 2) extended two-dimensional islands of the intercalate; and 3) three-dimensional Dumas–Herold domains [10]. In both the first and second cases HNO_3 molecules are randomly distributed in the HOPG. The third form, built up from intercalate islands, is ordered along the c-axis. However, in our case the increase of σ_a immediately after the reaction begins rules out forms 1 and 2 of intercalation and, together with X-ray diffraction data, testifies that form 3 of intercalation takes place.

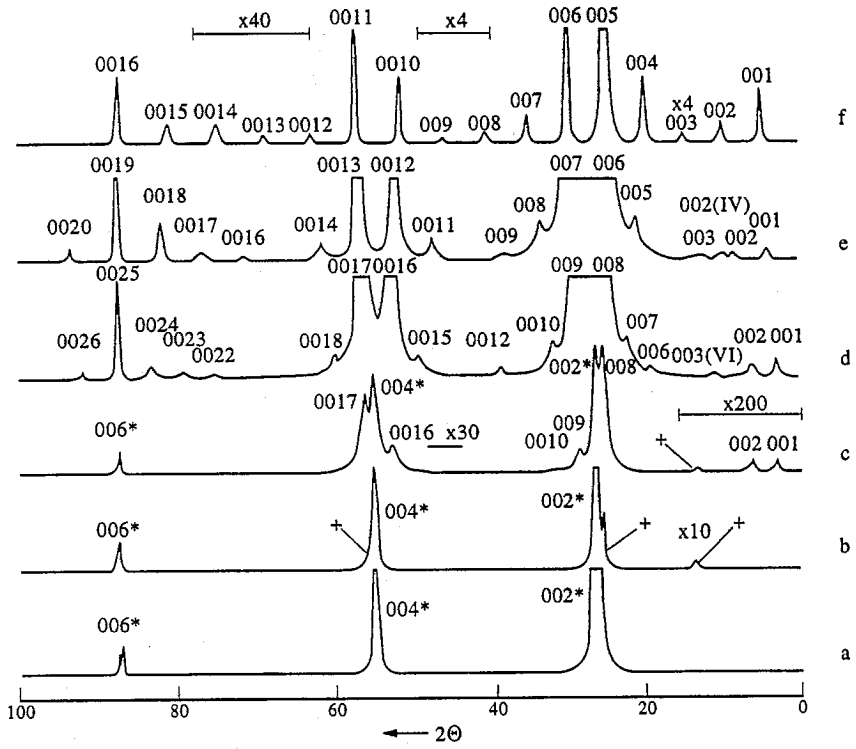

Fig. 3. (HOPG + HNO_3) system (001) X-ray diffractograms (CuK_α radiation) vs exposure time (τ) in HNO_3 atmosphere; $h \times l \times d = 0.4 \times 0.4 \times 0.026\,cm^3$. Diffractograms a–f correspond to the times marked by the arrows under the same letters in Fig. 4. In a, b and c the graphite and 'additional' reflections are designated by the symbols * and +, respectively. In c all reflections, excluding those designated by symbols * and +, correspond to the seventh stage. In d reflection 003(VI) corresponds to the sixth stage and other reflections to the seventh stage. In e reflection 002(IV) corresponds to the fourth stage and other reflections to the fifth stage. In f all reflections correspond to the fourth stage.

At $c||H_0$ the MWF penetrates into the HOPG plates mainly through its lateral sides, which are simultaneously parallel to both the c-axis and H_{rf} [8], in our case through the lateral sides ($h \times d$). Therefore, the evolution of the CESR spectra of the samples investigated is mainly due to variations of the composition and properties of the HOPG plate at the surface areas from the lateral sides with thickness of the order of δ_c.

To understand the nature of the observed CESR spectrum transformation of the (HOPG + HNO_3) system, it is necessary to note that the dependence of the shape and intensity of the CESR line on exposure time of samples in HNO_3 vapour is qualitatively identical to that of the CESR lineshape and intensity of the conductive substrate on the thickness of a spray-coated film of another metals [11]. It allows us to make

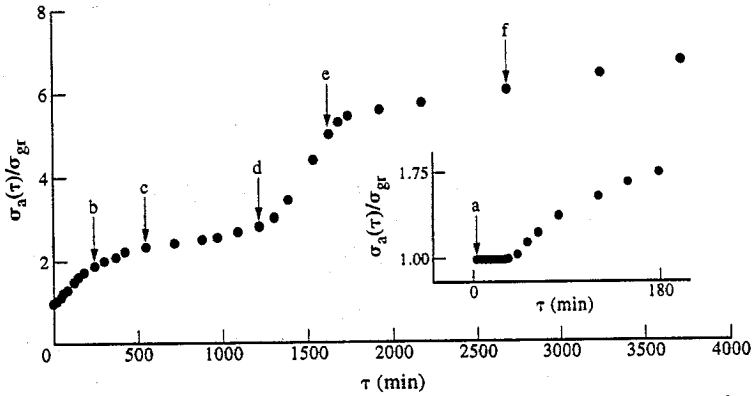

Fig. 4. Basal plane conductivity (σ_a) of HOPG plates with dimensions $h \times l \times d = 0.4 \times 0.4 \times 0.026\,cm^3$ vs exposure time (τ) in HNO_3 atmosphere. Arrows a–f mark the time at which the (001) X-ray diffractograms of a similar (HOPG + HNO_3) system were measured (see Fig. 3). σ_{gr} is the basal plane conductivity of a standard HOPG plate; $T = 300\,K$.

the conclusion that variations of shape and intensity of the HOPG CESR line are determined by the formation of a macroscopic 'intercalation' layer on the HOPG substrate, and by the advance of the boundary which separates the intercalated and the unintercalated HOPG.

Comparison of the evolution of the CESR spectra and (001) X-ray diffraction pictures of the HOPG plates with unprotected and protected basal planes suggests that there are two different intercalation mechanisms: 1) the slow diffusion of the intercalate through sides which are parallel to the c-axis, in the whole sample thickness; and 2) relatively fast nucleation of a new phase in the near surface galleries.

In the HOPG plates with protected basal planes only the first of the above-mentioned intercalation mechanisms is effective. That is why: 1) the graphite CESR signal from the plate basal sides is observed up to the completion of intercalation along l (i.e. until contact of the antiparallel fronts of intercalation); 2) before the end of the first intercalation phase the graphite CESR signal has an A/B ratio which is characteristic for localized spins; and 3) the additional reflections are absent in the (001) X-ray diffraction picture.

In the HOPG plates with unprotected basal planes, both intercalation mechanisms are effective. In this case the filling of the near surface galleries on a thickness more than δ_a (where $\delta_a = 4.7 \times 10^{-4}$ cm is the skin-depth corresponding to σ_a in the X-band) is accomplished faster than the intercalate diffusion along the galleries, which are distant from the basal surface, on a thickness δ_c. That is why, in the case under consideration: 1) the graphite CESR signal disappears earlier than in the experiments with plates which have protected basal planes; and 2) in the 'induction' period the new (001) X-ray reflections ('additional' reflections) were observed.

The presence of the low and high limit value of the induction period vs sample thickness dependence shows that each of the intercalation mechanisms has its own value of τ_i.

The constancy of ΔH^* from as soon as this signal is first registered up to $\Delta\tau_1$ in sample 1 testifies that, in this time interval, in the intercalated regions of the HOPG, on average, the stage and the interlayer packing of the intercalate are preserved.

Palchan *et al.* [3] suggested a procedure for determination of the intercalate two-dimensional diffusion constant D_{int}, by computer simulation of the experimental dependence $A/B(t)$ of the HOPG CESR line for the plates with unprotected basal planes. These simulations are based on the experimental facts that the A/B ratio of the HOPG plates differs insignificantly from A/B for the localized spins, and that the δ_c value in HOPG plates is comparatively large. Therefore, the HOPG spin carriers were considered to be localized. Then, for the description of the HOPG CESR lineshape evolution, the expressions obtained by Zevin and Suss [11] were used. These expressions describe the CESR lineshape of localized paramagnetic ions in a substrate with the film of another metal of varying thickness sprayed on the substrate. Later [8] we reinvestigated the CESR lineshape of the HOPG plates in detail, and established that the mobility of spins in the HOPG is higher than was reasoned before (and in particular in refs [12] and [13]) by approximately one order of magnitude. This result has cast some doubt on the possibility of D_{int} determination according to the procedure recommended in ref. [3]. Nevertheless, the D_{int} can readily be obtained from an analysis of the CESR spectrum evolution for the HOPG plates with protected basal planes. In reality, if we know the characteristic time interval Δt from the beginning of the CESR line transformation up to the disappearance of the CESR signal which is observed only from basal planes, we can estimate the two-dimensional intercalate diffusion constant using the well-known formula $D_{int} = \chi^2/2\Delta t$, where $x = l/2$ and $\Delta t = 13$ h. In this case $D_{int} \sim 2.6 \times 10^{-5}$ cm^2 min^{-1}. The latter value of D_{int} is approximately an order higher than that determined by Palchan *et al.* [3].

The intercalation process is accompanied by a stepwise increase of the spin carrier content (Fig. 2(b)). According to the (001) X-ray diffraction data, each plateau of the $I^*(t)$ dependence is associated with a definite stage of HNO_3 GICs. In this case, the time which is required for advance of the stage-change front from the lateral edge of the plate (where the new stages are nucleated) to make contact with the antiparallel front of this transformation, can be estimated if we know the time interval between the end of one plateau and the onset of the following one. In our case (Fig. 2(b)) this time, for instance, for the stage change between 6 and 5 is, approximately, equal to 0.4 h. Consequently, the rate of motion of the interface between stages is, approximately, equal to 8.3×10^{-4} cm min^{-1}.

It should be emphasized that during the time interval in which I^* is nearly constant, the smooth decrease in ΔH^* continues (Fig. 2(b)). That is, on the $I^*(t)$ plateau, the change of interlayer arrangement of the intercalate continues without a stage change. In particular, this ΔH^* decrease may reflect the process of growth of the intercalate islands as their number in the graphite galleries increases.

In summary, in this paper we present the results of *in situ* CESR, contactless conductivity, and X-ray diffraction studies of earlier unknown aspects of the intercalation process of HNO_3 molecules into HOPG plates with different dimensions. The application of a new procedure in this experiment allows us to

determine and study some individual reaction steps, two essentially different intercalation mechanisms, and constants of the two-dimensional diffusion of the intercalate, as well as allowing us to estimate the velocity of the advance of the stage index change front occurring at the interface between the initial stage and the next stage.

Acknowledgements—The authors are grateful to L. B. Nepomnyashchii (State Research Institute of Graphite, Moscow) for the HOPG plates used in the synthesis of GIC. This work was supported by a grant from the Russian Foundation of Basic Research (N 97-03-33346a).

REFERENCES

1. Dresselhaus, M. S. and Dresselhaus, G., *Adv. Phys.*, 1981, **30**, 139.
2. Davidov, R., Milo, O., Palchan, I. and Selig, H., *Synth. Met.*, 1983, **8**, 83.
3. Palchan, I., Davidov, D., Zevin, V. and Polatsek, G., *Phys. Rev. B*, 1985, **32**, 5554.
4. Palchan, I., Mustachi, F., Davidov, D. and Selig, M., *Synth. Met.*, 1984/85, **10**, 101.
5. Nakajima, M., Kawamura, K. and Tsuzuku, T., *J. Phys. Soc. Jpn*, 1988, **57**, 1572.
6. Ziatdinov, A. M., Tsvetnikov, A. K., Mishchenko, N. M. and Sereda, V. V., *Mat. Sci. Forum*, 1992, **91/93**, 563.
7. Pendrys, L. A., Zeller, C. and Vogel, F. L., *J. Mat. Sci.*, 1980, **15**, 2103.
8. Ziatdinov, A. M. and Mishchenko, N. M., *Fiz. Tverdogo Tela (Russia)*, 1994, **36**, 2360.
9. Dyson, F. J., *Phys. Rev.*, 1955, **98**, 349.
10. Dumas, N. and Herold, A., *C. R. Acad. Sci. Paris Series C*, 1969, **268**, 373.
11. Zevin, V. and Suss, J. T., *Phys. Rev. B*, 1986, **34**, 7260.
12. Wagoner, G., *Phys. Rev.*, 1960, **118**, 647.
13. Stein, R. M., Walmsley, L. and Rettori, C., *Phys. Rev.*, 1985, **32**, 4134.